

New red giants in NGC 6791 and NGC 6819 using *Kepler* superstamps

A. Covelo-Paz^{1,2,3}, N. Themeßl^{2,3}, F. Espinoza-Rojas^{2,3}, and S. Hekker^{2,3}

¹ Department of Astronomy, University of Geneva, Chemin Pegasi 51, 1290 Versoix, Switzerland
e-mail: alba.covelopaz@unige.ch

² Center for Astronomy, Landessternwarte (ZAH/LSW), Heidelberg University, Königstuhl 12, 69117 Heidelberg, Germany

³ Heidelberg Institute for Theoretical Studies (HITS), Schloss-Wolfsbrunnenweg 35, 69118 Heidelberg, Germany

Received XX; accepted YY

ABSTRACT

Context. Stars that are members of stellar clusters are assumed to be formed at the same time and place from material with the same initial chemical composition. These additional constraints on the ensemble of cluster stars make these stars suitable as benchmarks.

Aims. We aimed 1) to identify previously unknown red giants in the open clusters NGC 6791 and NGC 6819, 2) to extract their asteroseismic parameters, and 3) to determine their cluster membership.

Methods. We followed a dedicated method based on difference imaging to extract the light curves of potential red giants in NGC 6791 and NGC 6819 from *Kepler* superstamp data. We extracted the asteroseismic parameters of the stars that showed solar-like oscillations. We performed an asteroseismic membership study to identify which of these stars are likely to be cluster members.

Results. We found 149 red giant stars within the *Kepler* superstamps, 93 of which are likely cluster members. We were able to find 29 red giants that are not primary targets of *Kepler*, and therefore, their light curves had not been released previously. Five of these previously unknown red giants have a cluster membership probability greater than 95%.

Key words. asteroseismology – open clusters and associations: individual (NGC 6791, NGC 6819) – stars: solar-type – techniques: photometric

1. Introduction

Open clusters are remarkable features in the Milky Way. They contain up to a few thousand stars that are thought to have formed at the same time from the same molecular cloud. Hence, stars in clusters are assumed to have similar properties, such as age, initial chemical composition, and distance. Due to these shared initial conditions, studying the properties of cluster stars at different evolutionary stages allows us to constrain and test theories of stellar evolution and to gain insights into the formation and chemical evolution of our own Galaxy (e.g. [Vandenbergh 1983](#); [Salaris 2013](#); [Cantat-Gaudin & Anders 2020](#)). In this study, we search for additional oscillating red giants in the open clusters NGC 6791 and NGC 6819, which were observed by the *Kepler* space mission ([Borucki et al. 2009](#); [Gilliland et al. 2010](#)).

Kepler observed the same field in the sky for four years. From the $\sim 500\,000$ stars in the field that are brighter than the targeted threshold (<16 mag in the *Kepler* passband; [Batalha et al. 2010](#)), $\sim 150\,000$ stars were selected as primary targets for the mission. They are a subset of the *Kepler* Input Catalog (KIC; [Brown et al. 2011](#)). The *Kepler* field of view contains four open clusters: NGC 6791, NGC 6811, NGC 6819, and NGC 6866. Two of them, NGC 6791 and NGC 6819 (~ 8.5 and ~ 2.5 Gyr old, respectively; [Basu et al. 2011](#)), were found to contain a substantial number of oscillating red giant stars, and ~ 120 have been targeted by the *Kepler* mission and were studied with asteroseismology based on these data. For these stars, studies have determined asteroseismic parameters, stellar properties such as mass and radii ([Hekker et al. 2011a](#)), evolutionary stage ([Corsaro et al.](#)

[2012](#)), mass loss ([Miglio et al. 2012](#)), helium content ([McKeever et al. 2019](#)), core mixing ([Bossini et al. 2017](#)), stellar ages ([Basu et al. 2011](#)), and cluster membership ([Stello et al. 2011](#)). However, these clusters are likely to contain more oscillating stars that have not yet been analyzed.

Asteroseismology is a powerful technique that can probe the internal structure of stars through the study of their global oscillations. This method can be used to obtain global properties of red giant stars, such as stellar mass, radius, and evolutionary stage. To perform an asteroseismic analysis, it is necessary to obtain the light curve of the star. The mode of operation of *Kepler* was based on providing the light curves for only those stars that were observed as primary targets of the mission, that is, a subset of the KIC catalog. In addition to the target pixel files that were obtained for the preselected stars, the mission collected photometric data of the whole central regions of the open clusters NGC 6791 and NGC 6819. These data products are so-called superstamps that comprise long-cadence (~ 30 minutes) photometric observations with a spatial size of 200×200 pixels (13.3 arcminutes on one side). These data can be used to extract the light curve of any resolved star within the superstamps. Most of the stars in the open clusters NGC 6791 and NGC 6819 were not primarily targeted, and therefore, no light curves were released. We aim to extract the light curves of oscillating red giants from the superstamp data that were not primary targets of *Kepler*.

The light curve of a star can be extracted with different methods. The most commonly used technique is aperture photometry, which was successfully applied to the observed KIC stars and some superstamp stars (e.g. [Handberg & Lund 2014](#); [Lund](#)

et al. 2015). Aperture photometry is a reliable method for fairly isolated stars, but has its limits in highly crowded fields, for instance, central regions of open clusters or for saturated objects because it can introduce background signal. In contrast, difference imaging is a preferred technique for probing crowded fields because it removes all nonvariable signal that neighboring stars might be introducing. A light-curve extraction method based on difference imaging was implemented by Colman et al. (2022). They successfully tested their *IRIS* pipeline on KIC targets that are located within the *Kepler* superstamp data.

We used the method developed by Colman et al. (2022) to extract the light curves of red giant stars from the *Kepler* open cluster superstamp data of NGC 6791 and NGC 6819. We selected ~ 500 stars in the superstamps that are potential cluster red giants. We did this using colors and magnitudes from *Gaia* data (eDR3; Gaia Collaboration et al. 2021), and distances derived by Bailer-Jones et al. (2021). About half of the selected stars were not primary targets of *Kepler*, and their light curves were not previously extracted. We downloaded the uncorrected light curves of the KIC targets in our sample, extracted by Colman et al. (2022), and applied the *IRIS* pipeline to the non-KIC targets. We corrected the light curves using a modified version of the KASOC correction filter (Handberg & Lund 2014). We performed an asteroseismic analysis including cluster membership study of those stars that showed solar-like oscillations.

2. Target selection

We focused on the open clusters NGC 6791 and NGC 6819, which are known to host a substantial number of red giant stars. The *Kepler* mission provided high-quality photometric data for these clusters over a time span of four years. These superstamp data enable an asteroseismic analysis of any resolved star within the central regions of the clusters, including stars that were not primary targets of the mission.

First, we computed the expected number of red giant stars in these clusters that are observable with *Kepler*. Based on color-magnitude data from ground-based cluster surveys (Stetson et al. 2003; Hole et al. 2009; Ak et al. 2016), we selected the stars that are likely to be red giants according to their location in the color-magnitude diagram. We only considered stars with a V magnitude below 16.7, as we do not expect to find oscillations in fainter red giants (Stello et al. 2011). We found ~ 200 and ~ 150 observable red giants in NGC 6791 and NGC 6819, respectively. So far, asteroseismic studies have focused on ~ 120 oscillating red giants in total in these clusters, potentially leaving several dozen stars to be studied.

To find these cluster red giant stars, we selected all the stars in the superstamps that are within the published color, magnitude, and distance ranges of the confirmed cluster red giants (Stello et al. 2011). We obtained the colors and magnitudes for these reference stars from *Gaia* eDR3. We used the *gaia-kepler.fun* crossmatch database¹ to determine their *Gaia* identification numbers from the KIC numbers provided by Stello et al. (2011). We took distance measurements provided by Bailer-Jones et al. (2021) that were derived based on *Gaia* eDR3 parallaxes. The intervals of color, magnitude, and distance that we obtained for cluster red giants are shown in table 1.

We searched the *Gaia* eDR3 catalog for stars that fulfilled these criteria within the superstamp regions. We obtained a list of 281 candidate red giants in NGC 6791 and 232 in NGC 6819. These are more than the ~ 200 and ~ 150 observable red giants

Table 1. Intervals applied to our target selection.

Cluster	Color ($bp - rp$)	<i>Gaia</i> (mag)	Distance (pc)
NGC 6791	1 – 2.5	12 – 17	2 500 – 5 500
NGC 6819	0.8 – 2.5	10 – 15	1 000 – 4 200

Notes. Color, magnitude, and distance ranges for the confirmed cluster red giants in Stello et al. (2011).

that we expect in each cluster. Therefore, it is likely that a subset of these candidates are not red giant stars. Figures 1 and 2 show the positions of these candidates within the superstamps. Out of these stars, 225 are not primary targets of *Kepler*, and their light curves have not been released so far.

3. Light-curve extraction

The *Kepler* superstamps contain long-cadence (~ 30 minutes; Jenkins et al. 2010) photometric data for stars in NGC 6791 and NGC 6819, obtained during the observing quarters 1-17 of the mission. This results in over four years of data for both clusters. No observations are available for NGC 6819 during quarters 6, 10, and 14, due to a broken CCD.

To extract the light curves of the selected stars from the superstamps, we applied the *IRIS* pipeline (Colman et al. 2022), which is based on a difference-imaging method. The pipeline starts by cutting out a 5×5 pixel postage stamp from the superstamp with the target star at the center. This places the data in a format similar to a *Kepler* target pixel file, that is, a time series of pixel images that contains all the photometric data of the star that were obtained during a given quarter. The code then estimates the crowding of the region around the star by comparing the total magnitude of the frame-averaged postage stamp to the known *Kepler* magnitude of the star. If the two magnitudes are similar, the star is fairly isolated. However, if the postage magnitude is lower than the magnitude of the star (i.e., the postage-stamp flux is higher than the flux of the star), it is likely that a nearby star contaminates the data. Because *Kepler* magnitudes are only available for primary targets of the mission (Brown et al. 2011), we instead estimated the crowding using *Gaia* magnitudes because the two missions used similar passbands. Then, the 5×5 pixel postage stamp is resampled by a factor of 20 to 100×100 pixels using bilinear interpolation in order to create more precise apertures for the stars (see Fig. 3). Next, an aperture mask is defined as a 2D Gaussian function with a width based on the crowding of the region. Apertures for isolated stars have a larger width than those for stars with crowded backgrounds. This reduces the contamination of nearby stars in crowded regions. Difference imaging is then applied to the 100×100 pixel stamps by subtracting the frame-averaged image from each frame in the stamps. This removes all the flux sources that are not variable. Finally, the flux is extracted from each frame by applying the aperture mask. The result is a light curve for a single quarter that only accounts for variable sources.

The light curves of the KIC targets in our sample have already been extracted using the *IRIS* method by Colman et al. (2022). Thus, we downloaded the uncorrected light curves of the KIC stars and used the *IRIS* pipeline to extract those of the non-KIC targets. After extracting each light curve, we applied a number of corrections to remove systematics introduced by the instrument and the mission. We applied the KASOC filter (Handberg & Lund 2014), which was designed to correct *Kepler* light curves obtained with aperture photometry. This pipeline uses the

¹ <https://gaia-kepler.fun/>

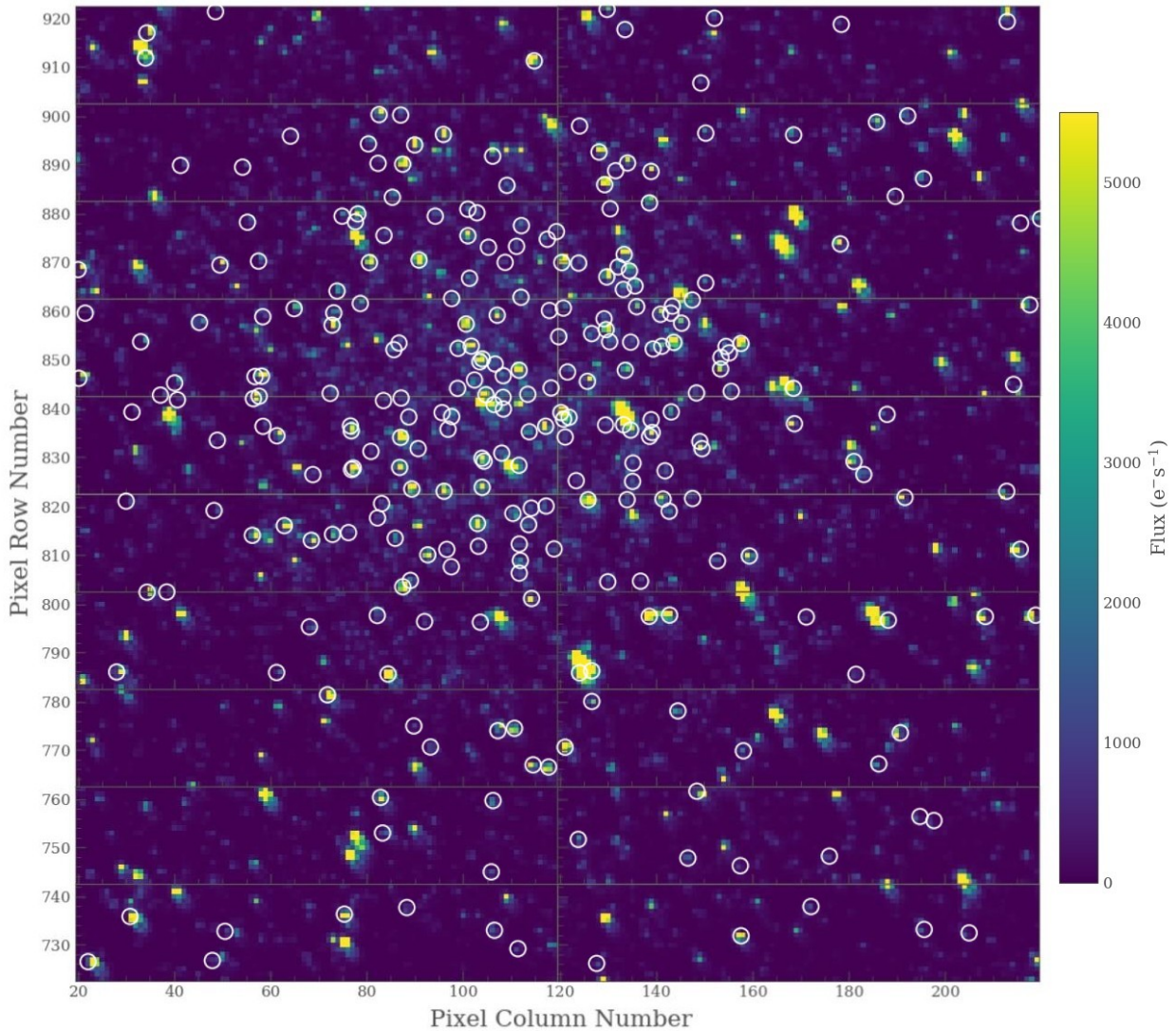


Fig. 1. Cluster superstamp of NGC 6791. These data were released as 20 substamps. We selected 281 stars as red giant candidates (encircled).

quality flags released by the mission and removes data points that are flagged as desaturation events, manual exclusions, and arg-brightening. Furthermore, it corrects for the jumps in the light curve that are produced by attitude tweaks. Other quality flags are ignored. However, we realized that safe modes and Earth points produced significant jumps in our light curves. Therefore, we extended the jump corrections to data points showing these quality flags. Then, the pipeline filtered the light curve for long-term trends (i.e., instrumental drifts and stellar activity) and short-term trends (i.e., transit features and instrumental effects, e.g., sudden jumps after safe modes), giving each filter a different weight depending on the relative standard deviation of the signal. Last, we performed sigma clipping to remove all data points that deviated by more than 5σ from the average. The resulting light curves showed significantly diminished systematic effects.

After we obtained the corrected light curves of the star for every observed quarter, we normalized the flux to be shown in parts per million. Last, we appended the normalized light curves of each quarter to produce the final light curve.

The resulting light curves of the red giants in our catalog that show oscillations are available on GitHub².

² <https://github.com/astroalba/kepler-red-giants-lc>

4. Asteroseismic analysis

We computed a power density spectrum for each star from the extracted light curves with the aim of detecting solar-like oscillations. The power density spectrum of a red giant star shows a distinct power excess that comprises the oscillation modes. To identify this potential power excess, we first implemented the automated CV method following Bell et al. (2019). This method is based on the coefficients of variation (CV), that is, the ratio of the standard deviation of the power to its mean. This ratio should be equal to 1 in the presence of χ^2 noise statistics as expected for the power density spectrum of solar-like oscillators. Any signal that is not caused by stochastic noise will present higher CV values. An expected width of the oscillatory signal in the CV method as a function of the frequency of maximum oscillation power (ν_{\max}) was introduced based on the analysis of the stars in the APOKASC-DR2 (Pinsonneault et al. 2018). We found 59 solar-like oscillators and 44 stars with ambiguous results. After visual inspection of the latter, we confirmed 46 oscillations that the CV method could not clearly detect, probably due to changes in the statistics of the power density spectrum due to contamination of neighboring stars. Combining this with oscillating red giants from the literature and a final visual inspection, we identified a

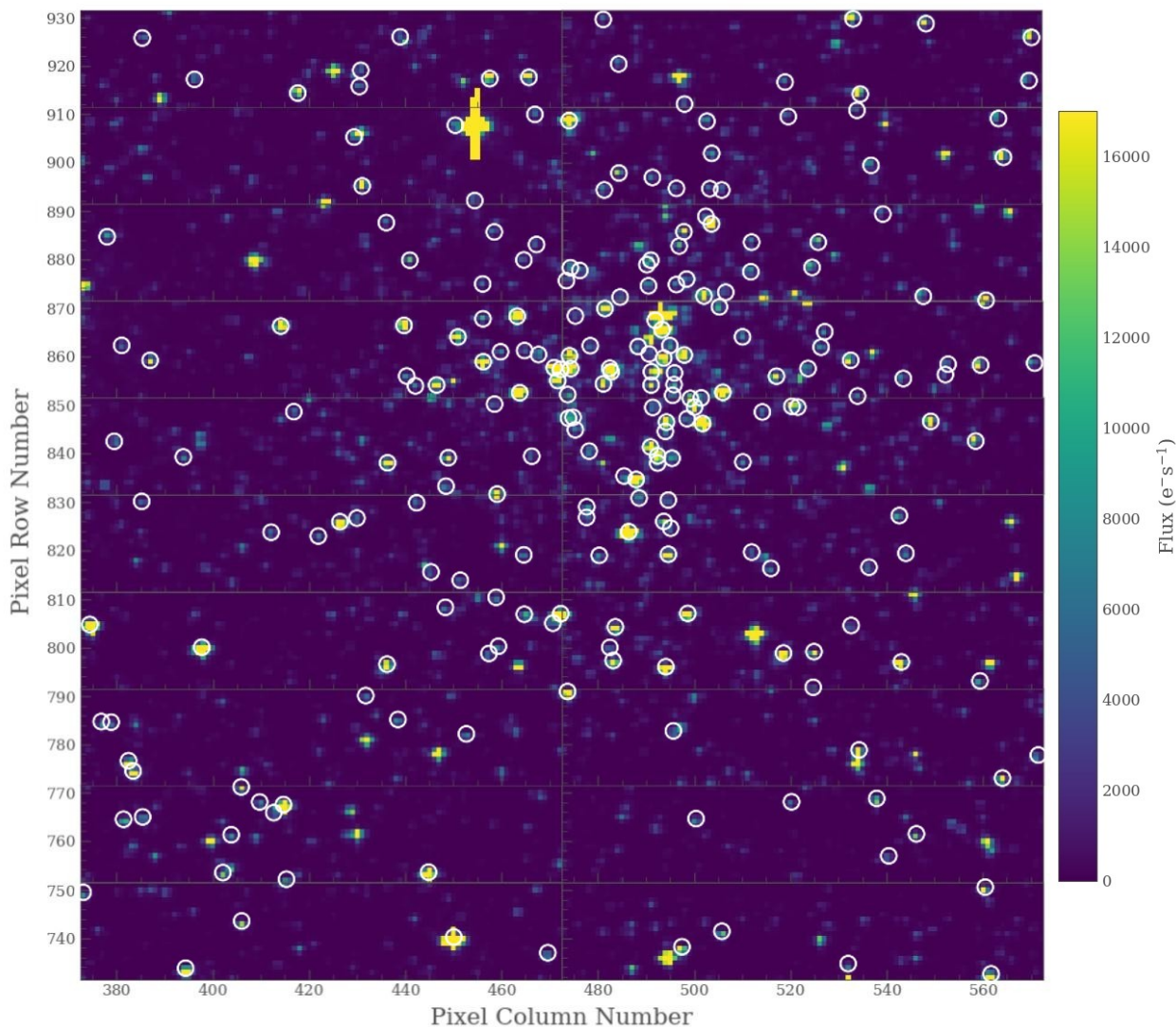


Fig. 2. Same as Fig. 1, now for NGC 6819. We selected 232 stars as red giant candidates (encircled).

final sample of 149 oscillating red giants, (91 in NGC 6791 and 58 in NGC 6819) in our set of 513 stars.

For these 149 oscillating stars, we performed an asteroseismic analysis and extracted the frequency of their maximum oscillation power (ν_{\max}) using the code called tools for the automated characterization of oscillations (TACO) (Hekker et al. in prep.). We obtained ν_{\max} from a global fit to the power density spectrum through a Bayesian Markov chain Monte Carlo framework. The model consists of three granulation components, one white-noise term, and a Gaussian fit to the power excess comprising ν_{\max} . We took the 50th percentile from the posterior ν_{\max} distribution as the final parameter estimate and the 16th and 84th percentiles as its uncertainties. In Figure 4 we show a power density spectrum with the global fit. We report the *Gaia* eDR3 *G* magnitudes and the measured ν_{\max} values for the oscillating red giant stars in the field of view of NGC 6791 and NGC 6819 in tables A.1 and A.2.

Out of the 149 oscillating red giants, 83 were previously analyzed by Corsaro et al. (2012). They obtained asteroseismic parameters, including ν_{\max} , for 115 oscillating red giant stars in the *Kepler* open clusters. At the time, only seven quarters of *Kepler* data were available, which corresponds to a time stamp of ~ 19 months (less than half of the data that are currently available).

A comparison between our results and theirs is shown in figure 5. Although the two results agree for most stars (with a sigma-clipped scatter of 4, in line with earlier works; e.g. Hekker et al. 2011b), there are a few stars with very different values of ν_{\max} as a result of the two methods. These outliers seem to have picked up an entirely different signal on the power density spectrum. This might be due to differences in the methods used for light-curve extraction and correction.

5. Cluster membership study

We performed an asteroseismic cluster membership study to identify the oscillating stars that belong to NGC 6791 and NGC 6819. Following the approach introduced by Stello et al. (2010), we used the ν_{\max} measurements together with the *Gaia* *G* magnitudes to determine the most likely cluster members. We note here that the *G* passband covers a wavelength range of about 330 – 1050 nm, which is similar to the 2MASS passbands used by Stello et al. (2010).

For red giant stars, the asteroseismic parameter ν_{\max} is related to the global properties of the star through a scaling relation

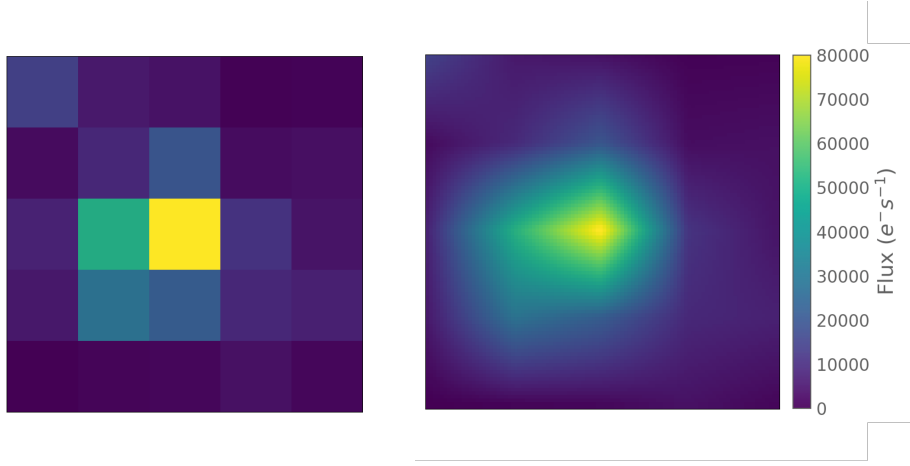


Fig. 3. Resampling of the pixel stamps with the *IRIS* code. Left: 5×5 pixel stamp of one of the target stars in NGC 6819. Right: 100×100 pixel stamp of the same star, obtained after resampling the original stamp by a factor of 20 using bilinear interpolation.

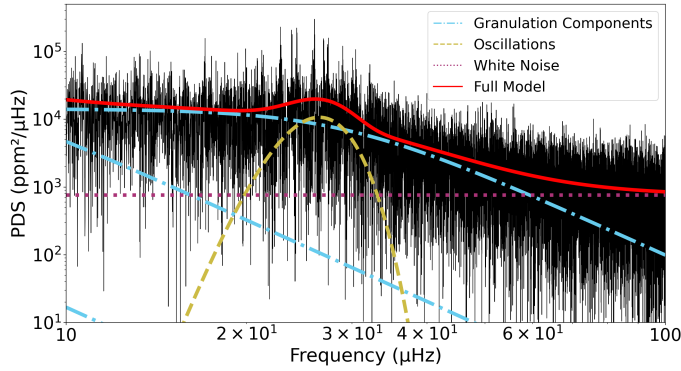


Fig. 4. Power density spectrum (in black) of one of the target stars in NGC 6791 (star 39 in table 1). The solid red line shows the global model fit computed by TACO, which includes three granulation components (dashed blue lines), one white-noise component (horizontal dotted magenta line), and a Gaussian fit to the oscillation power excess (dashed yellow line).

(Brown et al. 1991; Kjeldsen & Bedding 1995),

$$\nu_{\max} \simeq \frac{M/M_{\odot}(T_{\text{eff}}/T_{\text{eff},\odot})^{3.5}}{L/L_{\odot}} \nu_{\max,\odot}, \quad (1)$$

where M , T_{eff} , and L are the mass, effective temperature, and luminosity of the star. The nominal effective temperature of the Sun is $T_{\text{eff},\odot} = 5772 \text{ K}$ (Prša et al. 2016), and $\nu_{\max,\odot} = 3100 \mu\text{Hz}$ (Basu et al. 2010) is a reference value that scales the relation to the Sun.

For red giant stars, the stellar masses and effective temperatures vary only marginally compared to the luminosities, which have a wider range of values when these stars evolve. Thus, there is a tight correlation between ν_{\max} and the stellar luminosity. For cluster red giants, this translates into a correlation between ν_{\max} and the apparent stellar magnitude because all the stars are assumed to be located at a similar distance. By plotting the apparent magnitude versus ν_{\max} , cluster red giants line up, while foreground and background stars deviate from the correlation.

In Figure 6 we show the measured asteroseismic ν_{\max} values versus the published *Gaia* G magnitudes for our stars with detected solar-like oscillations in NGC 6791 (top) and NGC 6819 (bottom). In each diagram, we indicate the confidence region (dashed lines) hosting stars with a 95% confidence to be part

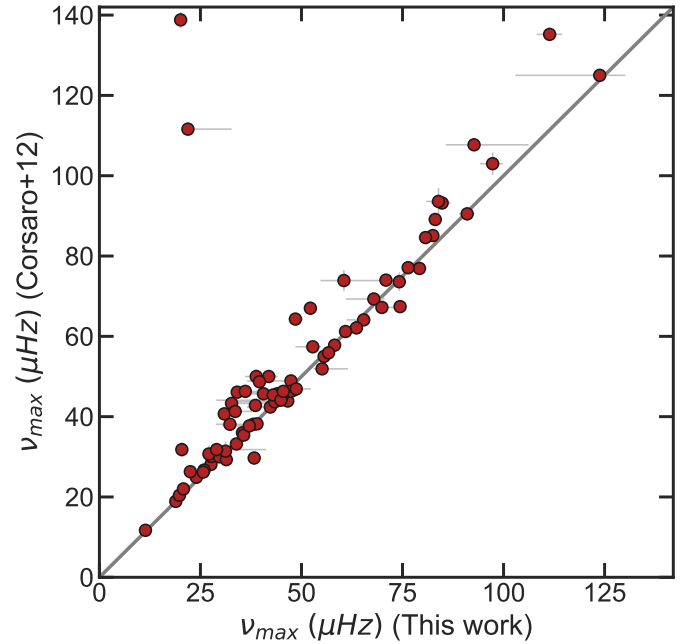


Fig. 5. Comparisons of the frequencies of maximum oscillation (ν_{\max}) that we obtained to those released by Corsaro et al. (2012).

of the cluster population. The confidence intervals for each cluster were computed around a linear regression line based on ν_{\max} values, G magnitudes, and their respective uncertainties for a set of preselected KIC open cluster red giants that were studied by Stello et al. (2010). Their cluster memberships were independently confirmed through asteroseismic, radial velocity, and proper motion studies. The cluster membership probabilities of stars outside the 95% confidence intervals decrease with increasing distance to the confidence region.

Using this method, we found that 93 red giants have an asteroseismic cluster membership probability of more than 95% (61 in NGC 6791 and 32 in NGC 6819). Of these, 5 stars are not primary targets of *Kepler*, and they are confirmed to be cluster members using an asteroseismic analysis for the first time here. Figure 7 shows the positions of these oscillating cluster red giants within their respective clusters.

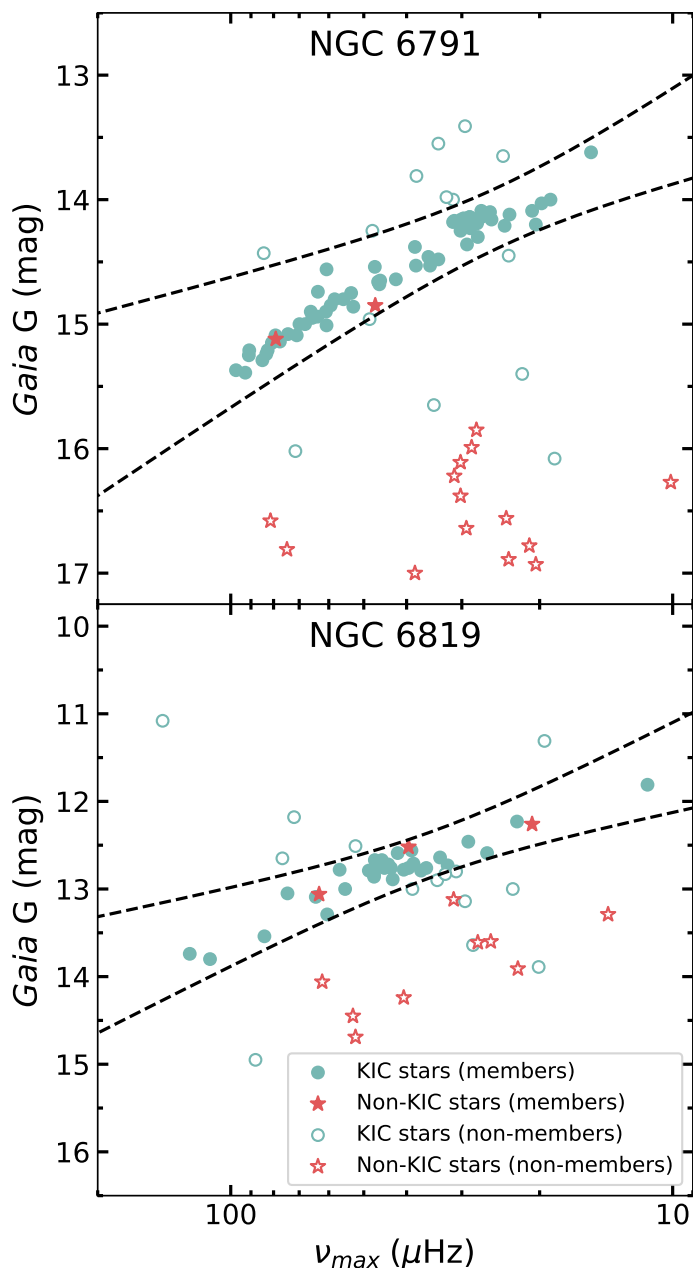


Fig. 6. *Gaia* G magnitude vs. frequency of the maximum oscillation power ν_{\max} for red giants in NGC 6791 and NGC 6819. Dots are KIC stars, and star symbols are newly detected stars. Filled symbols are likely to be cluster members, and open symbols are nonmembers. The axes are oriented to make the plot similar to a color-magnitude diagram. The dashed lines show the regions in which cluster stars tend to line up in these diagrams and their 95% confidence intervals.

Because we expect these clusters to host ~ 200 and ~ 150 observable red giant stars, respectively (see section 2), it is likely that we missed about three-quarters of the cluster red giants. This could be due to our restrictive selection in color, magnitude, and distance (see table 1), or due to limitations of our method for extracting the oscillations in the most crowded regions of the cluster, where the aperture masks are narrow in order to prevent contamination. It is also possible that we missed some oscillating stars due to a high level of noise in the power density spectrum, which would partially hide the oscillations.

An alternative method for determining cluster membership that does not rely on asteroseismology was presented by Cantat-

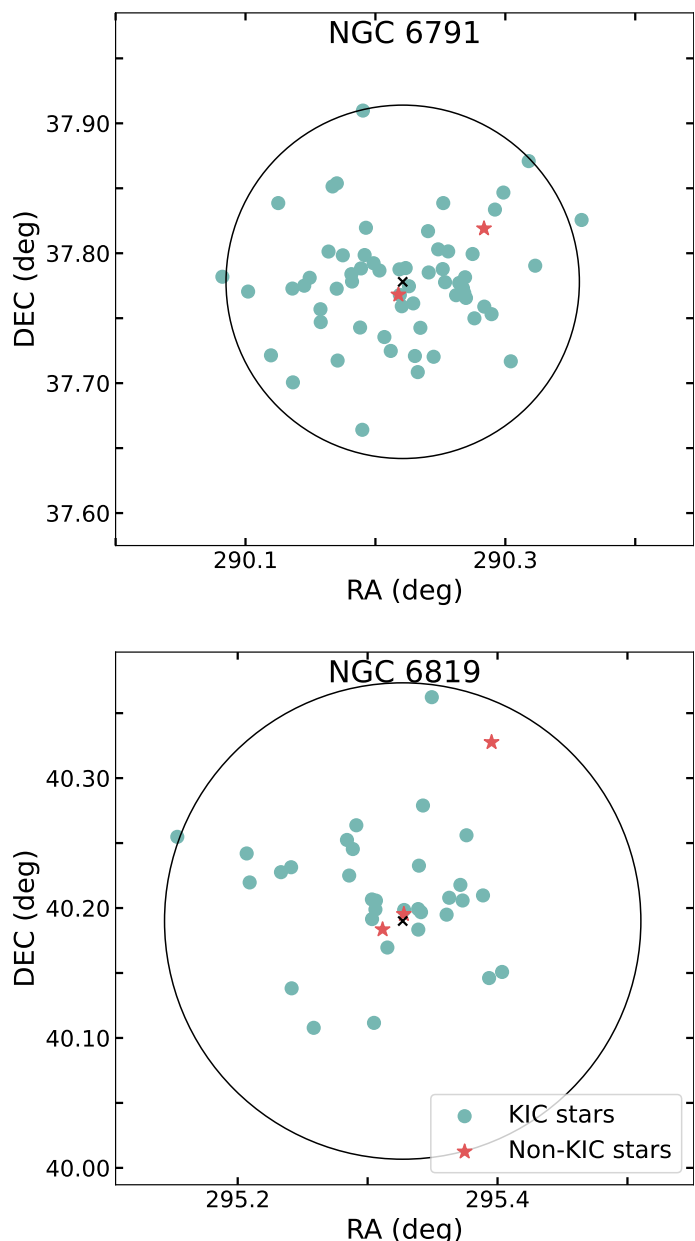


Fig. 7. Sky positions of the oscillating red giants that we found to be likely cluster members. Dots are KIC stars, and star symbols are newly detected stars. The large circles represent the approximate location of the clusters (Cantat-Gaudin & Anders 2020), and the central cross represents the cluster center.

Gaudin & Anders (2020). This method applies an unsupervised classification scheme using *Gaia* DR2 proper motions and parallaxes to compute membership probabilities. The authors studied 1481 stellar clusters in the Galactic disk, including NGC 6791 and NGC 6819, and provided a list of cluster stars and their membership probability. We added the membership determination from Cantat-Gaudin & Anders (2020) to tables A.1 and A.2 of our oscillating stars. Out of the 149 oscillating red giants that we detected, 113 are considered cluster members with a probability of 100% in their work, while our method retrieved 93 members with a probability of 95%. Thus, the two methods agree for most of the stars in our sample, except for $\sim 10\%$ of them. It seems that our method is much more restrictive in determining cluster membership, and we might be missing some members due to this.

6. Summary and conclusions

We have successfully extracted the light curves of 513 red giant candidates in the open clusters NGC 6791 and NGC 6819 using the superstamp data from *Kepler*. We were able to confirm that 149 of these stars are oscillating red giants, and we measured their frequency of maximum oscillation power (ν_{\max}). By performing an asteroseismic membership study, we found that 93 of these red giants are likely to be cluster members. 75 of these were previously reported to be cluster members by [Stello et al. \(2011\)](#) based on a similar membership determination method. 11 nonmember red giants in our sample were reported to be cluster members by [Stello et al. \(2011\)](#). This is probably because our membership determination method is based on the correlation between the *Gaia* magnitude of each star and its ν_{\max} , while they used the *K* magnitude against $\Delta\nu$. Although both strategies are based on the same principle, it is possible that there is some scatter between the two methods, which would explain the disagreement for the 11 stars. It is also worth noting that at the time, only four quarters of *Kepler* data were available, making their light curves four times shorter than those we extracted.

Out of the 149 oscillating red giants that we found, 29 are not primary targets of *Kepler*, and their light curves have not been released previously. We found that 5 of these red giants are asteroseismic cluster members.

The method that we followed to extract the light curves from the *Kepler* superstamps allowed us to obtain the asteroseismic parameters of stars that are very close to the cluster center, which would be very challenging for aperture photometry. This method cannot only be applied to solar-like oscillators, but also to any other star within the superstamp data. Moreover, it can be used to extract the light curves in any moderately crowded region as long as high-precision long-term photometric data are available.

In the upcoming PLATO mission, the provisional fields that are expected to be observed (LOPS2 and LOPN1) contain about 300 open clusters ([Nascimbeni et al. 2022](#)). Our method can be used to extract the light curves of cluster stars observed by PLATO and provides an opportunity of performing asteroseismic analyses on these clusters. These analyses would allow us to obtain the parameters of more clusters in the Milky Way, which in turn would bring us closer to understanding the nature of these objects in our Galaxy.

Acknowledgements. We acknowledge funding from the ERC Consolidator Grant DipolarSound (grant agreement # 101000296). This work was funded by the Deutsche Forschungsgemeinschaft (DFG, German Research Foundation) – Project-ID 138713538 – SFB 881 (“The Milky Way System”, subproject P02)

References

- Ak, T., Bostancı, Z. F., Yontan, T., et al. 2016, *Ap&SS*, 361, 126
 Bailer-Jones, C. A. L., Rybizki, J., Fouesneau, M., Demleitner, M., & Andrae, R. 2021, *AJ*, 161, 147
 Basu, S., Chaplin, W. J., & Elsworth, Y. 2010, *ApJ*, 710, 1596
 Basu, S., Grundahl, F., Stello, D., et al. 2011, *ApJ*, 729, L10
 Batalha, N. M., Borucki, W. J., Koch, D. G., et al. 2010, *ApJ*, 713, L109
 Bell, K. J., Hekker, S., & Kuzlewicz, J. S. 2019, *MNRAS*, 482, 616
 Borucki, W., Koch, D., Batalha, N., et al. 2009, in *Transiting Planets*, ed. F. Pont, D. Sasselov, & M. J. Holman, Vol. 253, 289–299
 Bossini, D., Miglio, A., Salaris, M., et al. 2017, *MNRAS*, 469, 4718
 Brown, T. M., Gilliland, R. L., Noyes, R. W., & Ramsey, L. W. 1991, *ApJ*, 368, 599
 Brown, T. M., Latham, D. W., Everett, M. E., & Esquerdo, G. A. 2011, *AJ*, 142, 112
 Cantat-Gaudin, T. & Anders, F. 2020, *A&A*, 633, A99
 Colman, I. L., Bedding, T. R., Huber, D., & Kjeldsen, H. 2022, *ApJS*, 258, 39
 Corsaro, E., Stello, D., Huber, D., et al. 2012, *ApJ*, 757, 190
 Gaia Collaboration, Smart, R. L., Sarro, L. M., et al. 2021, *A&A*, 649, A6

- Gilliland, R. L., Brown, T. M., Christensen-Dalsgaard, J., et al. 2010, *PASP*, 122, 131
 Handberg, R. & Lund, M. N. 2014, *MNRAS*, 445, 2698
 Hekker, S., Basu, S., Stello, D., et al. 2011a, *A&A*, 530, A100
 Hekker, S., Elsworth, Y., De Ridder, J., et al. 2011b, *A&A*, 525, A131
 Hole, K. T., Geller, A. M., Mathieu, R. D., et al. 2009, *AJ*, 138, 159
 Jenkins, J. M., Caldwell, D. A., Chandrasekaran, H., et al. 2010, *ApJ*, 713, L120
 Kjeldsen, H. & Bedding, T. R. 1995, *A&A*, 293, 87
 Lund, M. N., Handberg, R., Davies, G. R., Chaplin, W. J., & Jones, C. D. 2015, *ApJ*, 806, 30
 McKeever, J. M., Basu, S., & Corsaro, E. 2019, *ApJ*, 874, 180
 Miglio, A., Brogaard, K., Stello, D., et al. 2012, *MNRAS*, 419, 2077
 Nascimbeni, V., Piotto, G., Börner, A., et al. 2022, *A&A*, 658, A31
 Pinsonneault, M. H., Elsworth, Y. P., Tayar, J., et al. 2018, *ApJS*, 239, 32
 Prša, A., Harmanec, P., Torres, G., et al. 2016, *AJ*, 152, 41
 Salaris, M. 2013, in *Asteroseismology of Stellar Populations in the Milky Way*, 9
 Stello, D., Basu, S., Bruntt, H., et al. 2010, *ApJ*, 713, L182
 Stello, D., Meibom, S., Gilliland, R. L., et al. 2011, *ApJ*, 739, 13
 Stetson, P. B., Bruntt, H., & Grundahl, F. 2003, *PASP*, 115, 413
 Vandenberg, D. A. 1983, *ApJS*, 51, 29

Appendix A: Tables

Table A.1. Oscillating red giants in NGC 6791.

ID	KIC	RA (°)	DEC (°)	<i>Gaia</i> (mag)	ν_{\max} (μHz)	Member (this work)	S11 member	C20 member
1	-	290.1856	37.6687	16.93	$20.4^{+0.4}_{-0.6}$	No	-	-
2	-	290.3508	37.7717	16.27	$10.1^{+0.6}_{-0.3}$	No	-	Yes
3	-	290.2810	37.7486	16.89	$23.5^{+10.2}_{-1.9}$	No	-	Yes
4	-	290.2403	37.7394	16.38	$30.2^{+0.4}_{-0.5}$	No	-	-
5	-	290.2641	37.7722	16.06	$30.2^{+8.7}_{-1.0}$	No	-	Yes
6	-	290.2548	37.7754	16.56	$23.8^{+0.4}_{-0.2}$	No	-	Yes
7	-	290.2796	37.7958	16.22	$31.2^{+0.5}_{-0.7}$	No	-	Yes
8	-	290.2794	37.7974	16.78	$21.1^{+0.1}_{-0.04}$	No	-	Yes
9	-	290.1708	37.7726	15.85	$27.8^{+1.7}_{-11.0}$	No	-	Yes
10	-	290.0669	37.8447	17.00	$38.3^{+1.4}_{-1.4}$	No	-	-
11	-	290.2177	37.7681	14.85	$47.1^{+1.3}_{-1.5}$	Yes	-	-
12	-	290.2525	37.7804	16.64	$29.3^{+1.2}_{-1.3}$	No	-	Yes
13	-	290.2031	37.7875	15.99	$28.5^{+0.6}_{-1.7}$	No	-	Yes
14	-	290.2500	37.8004	16.81	$74.6^{+1.4}_{-1.9}$	No	-	Yes
15	-	290.2836	37.8190	15.12	$79.1^{+1.0}_{-2.5}$	Yes	-	Yes
16	-	290.2318	37.8126	16.58	$81.3^{+0.8}_{-13.1}$	No	-	Yes
17	-	290.1668	37.8011	16.08	$18.5^{+0.8}_{-2.1}$	No	-	-
18	2297384	290.1899	37.6641	14.21	$20.4^{+0.3}_{-0.3}$	Yes	Yes	Yes
19	2435987	290.0822	37.7819	14.53	$38.1^{+0.4}_{-0.4}$	Yes	Yes	Yes
20	2436097	290.1020	37.7705	14.66	$42.3^{+0.6}_{-5.8}$	Yes	Yes	Yes
21	2436209	290.1196	37.7214	14.80	$58.2^{+0.7}_{-1.0}$	Yes	Yes	Yes
22	2436332	290.1361	37.7728	14.30	$27.6^{+0.7}_{-0.5}$	Yes	Yes	Yes
23	2436334	290.1365	37.7006	14.78	$63.5^{+3.1}_{-7.3}$	Yes	-	Yes
24	2436417	290.1452	37.7750	14.10	$25.9^{+0.5}_{-0.4}$	Yes	Yes	Yes
25	2436458	290.1494	37.7811	14.53	$35.4^{+0.7}_{-0.3}$	Yes	Yes	Yes
26	2436540	290.1577	37.7569	14.86	$52.8^{+2.0}_{-4.3}$	Yes	Yes	Yes
27	2436543	290.1579	37.7470	14.12	$23.4^{+0.7}_{-0.7}$	Yes	-	Yes
28	2436593	290.1618	37.7430	15.40	$21.9^{+10.8}_{-1.1}$	No	Yes	Yes
29	2436608	290.1634	37.7437	14.45	$23.5^{+0.4}_{-0.4}$	No	-	Yes
30	2436682	290.1702	37.7727	14.14	$27.1^{+0.5}_{-0.5}$	Yes	-	Yes
31	2436688	290.1709	37.7174	15.09	$79.2^{+1.1}_{-1.0}$	Yes	Yes	Yes
32	2436732	290.1749	37.7984	14.14	$28.8^{+0.5}_{-1.8}$	Yes	Yes	Yes
33	2436814	290.1815	37.7839	14.21	$24.0^{+0.8}_{-0.4}$	Yes	Yes	Yes
34	2436824	290.1820	37.7782	14.48	$33.9^{+0.3}_{-0.3}$	Yes	Yes	Yes
35	2436900	290.1882	37.7428	14.46	$35.7^{+0.3}_{-0.4}$	Yes	Yes	Yes
36	2436912	290.1889	37.7883	14.18	$30.0^{+1.0}_{-1.0}$	Yes	Yes	Yes
37	2436935	290.1905	37.7406	15.65	$34.7^{+1.1}_{-3.9}$	No	-	Yes
38	2436944	290.1917	37.7986	14.17	$28.5^{+0.5}_{-0.5}$	Yes	Yes	-
39	2437040	290.1986	37.7923	14.16	$25.7^{+0.3}_{-0.3}$	Yes	Yes	Yes
40	2437103	290.2031	37.7867	14.38	$38.3^{+1.4}_{-1.4}$	Yes	Yes	Yes
41	2437164	290.2069	37.7355	14.16	$30.1^{+0.5}_{-0.7}$	Yes	-	Yes
42	2437240	290.2118	37.7248	14.65	$45.9^{+0.5}_{-1.0}$	Yes	Yes	Yes
43	2437267	290.2141	37.7751	13.81	$38.0^{+2.0}_{-1.5}$	No	-	Yes
44	2437296	290.2159	37.7800	16.02	$71.4^{+0.7}_{-0.7}$	No	-	Yes
45	2437325	290.2185	37.7876	15.29	$84.8^{+2.1}_{-2.7}$	Yes	Yes	Yes
46	2437327	290.2188	37.7679	14.85	$59.4^{+1.0}_{-0.9}$	Yes	-	Yes
47	2437353	290.2203	37.7592	14.14	$28.8^{+0.4}_{-0.5}$	Yes	Yes	Yes
48	2437402	290.2233	37.7886	14.66	$46.4^{+0.6}_{-0.6}$	Yes	Yes	Yes
49	2437444	290.2258	37.7746	14.00	$18.9^{+0.2}_{-0.3}$	Yes	Yes	Yes
50	2437488	290.2291	37.7614	14.95	$65.4^{+1.3}_{-4.2}$	Yes	Yes	Yes
51	2437507	290.2304	37.7209	14.03	$19.8^{+0.4}_{-0.3}$	Yes	Yes	Yes
52	2437539	290.2326	37.7085	14.54	$47.2^{+0.8}_{-12.7}$	Yes	-	Yes
53	2437564	290.2346	37.7426	14.23	$28.07^{+0.7}_{-0.6}$	Yes	Yes	Yes
54	2437589	290.2363	37.7187	14.25	$47.8^{+0.6}_{-0.6}$	No	Yes	Yes

Table A.1. continued.

ID	KIC	RA (°)	DEC (°)	<i>Gaia</i> (mag)	ν_{\max} (μHz)	Member (this work)	S11 member	C20 member
55	2437653	290.2410	37.7852	15.09	$70.9^{+1.0}_{-1.0}$	Yes	Yes	Yes
56	2437698	290.2448	37.7203	14.19	$27.7^{+0.7}_{-0.7}$	Yes	Yes	Yes
57	2437781	290.2518	37.7878	15.21	$82.5^{+1.6}_{-1.6}$	Yes	Yes	Yes
58	2437805	290.2536	37.7777	14.15	$29.7^{+0.6}_{-0.6}$	Yes	Yes	Yes
59	2437901	290.2621	37.7677	14.25	$30.2^{+0.4}_{-0.4}$	Yes	-	Yes
60	2437933	290.2645	37.7771	15.39	$92.7^{+13.5}_{-7.0}$	Yes	Yes	Yes
61	2437957	290.2674	37.7730	15.25	$91.0^{+1.8}_{-2.0}$	Yes	Yes	Yes
62	2437972	290.2684	37.7694	15.15	$80.7^{+0.8}_{-0.9}$	Yes	Yes	Yes
63	2437976	290.2690	37.7815	15.24	$83.1^{+1.5}_{-1.7}$	Yes	Yes	Yes
64	2437987	290.2697	37.7656	14.18	$31.4^{+0.6}_{-0.6}$	Yes	Yes	Yes
65	2438038	290.2748	37.7994	14.94	$63.6^{+0.6}_{-0.6}$	Yes	Yes	Yes
66	2438051	290.2762	37.7499	14.09	$27.1^{+0.5}_{-0.6}$	Yes	Yes	Yes
67	2438069	290.2777	37.7176	14.00	$31.4^{+1.1}_{-1.0}$	No	-	-
68	2438139	290.2836	37.7971	13.55	$33.9^{+1.0}_{-2.2}$	No	-	No (70%)
69	2438140	290.2838	37.7589	15.00	$67.9^{+2.7}_{-6.9}$	Yes	Yes	Yes
70	2438191	290.2894	37.7531	15.21	$90.8^{+1.9}_{-1.9}$	Yes	-	Yes
71	2438333	290.3042	37.7168	14.90	$60.9^{+0.9}_{-1.2}$	Yes	Yes	Yes
72	2438470	290.3230	37.7904	14.90	$65.9^{+0.6}_{-1.7}$	Yes	-	Yes
73	2568575	290.0295	37.8334	13.41	$29.5^{+3.6}_{-1.0}$	No	-	-
74	2569055	290.1252	37.8386	14.17	$31.2^{+1.1}_{-0.6}$	Yes	Yes	Yes
75	2569078	290.1288	37.8125	13.65	$24.2^{+0.3}_{-3.6}$	No	-	-
76	2569360	290.1639	37.8013	14.09	$20.8^{+0.3}_{-0.3}$	Yes	Yes	Yes
77	2569390	290.1670	37.8514	15.01	$60.7^{+1.1}_{-1.2}$	Yes	-	Yes
78	2569426	290.1703	37.8538	14.56	$60.7^{+2.7}_{-0.9}$	Yes	-	-
79	2569618	290.1927	37.8196	14.80	$55.6^{+0.5}_{-0.5}$	Yes	Yes	Yes
80	2570094	290.2405	37.8170	15.00	$69.9^{+4.2}_{-1.4}$	Yes	Yes	Yes
81	2570172	290.2483	37.8030	15.08	$74.2^{+0.7}_{-1.2}$	Yes	Yes	Yes
82	2570214	290.2522	37.8386	14.11	$26.1^{+1.1}_{-0.9}$	Yes	Yes	Yes
83	2570244	290.2560	37.8014	15.37	$97.3^{+2.6}_{-3.1}$	Yes	Yes	Yes
84	2570384	290.2752	37.8681	14.96	$48.5^{+1.8}_{-1.7}$	No	Yes	Yes
85	2570518	290.2920	37.8336	14.68	$46.1^{+0.6}_{-8.4}$	Yes	Yes	Yes
86	2570575	290.2985	37.8467	15.14	$77.4^{+1.0}_{-1.0}$	Yes	-	Yes
87	2570578	290.2990	37.8794	13.98	$32.5^{+1.0}_{-1.8}$	No	-	-
88	2570652	290.3113	37.8854	14.43	$84.2^{+0.8}_{-0.8}$	No	-	No (60%)
89	2570696	290.3180	37.8709	13.62	$15.3^{+0.2}_{-0.2}$	Yes	-	-
90	2570924	290.3587	37.8256	14.75	$53.4^{+0.5}_{-0.5}$	Yes	-	Yes
91	2707716	290.1904	37.9098	14.36	$29.2^{+1.1}_{-1.3}$	Yes	-	Yes

Notes. We report whether they are cluster members following our method (this work), and whether they were determined to be cluster members in [Stello et al. 2011](#) (S11) and [Cantat-Gaudin & Anders 2020](#) (C20; only when their membership probability is 100%).

Table A.2. Oscillating red giants in NGC 6819.

ID	KIC	RA (°)	DEC (°)	<i>Gaia</i> (mag)	ν_{\max} (μHz)	Member (this work)	S11 member	C20 member
92	-	295.2984	40.0901	13.60	$25.8^{+1.0}_{-1.2}$	No	-	-
93	-	295.2936	40.1458	14.06	$62.1^{+1.5}_{-1.6}$	No	-	-
94	-	295.2583	40.1445	14.24	$40.6^{+0.9}_{-0.9}$	No	-	-
95	-	295.2676	40.1656	13.61	$27.6^{+1.1}_{-0.6}$	No	-	-
96	-	295.3279	40.1953	12.26	$20.8^{+0.4}_{-0.5}$	Yes	-	No (60%)
97	-	295.2844	40.1772	13.29	$14.0^{+0.2}_{-0.2}$	No	-	-
98	-	295.3115	40.1835	12.52	$39.6^{+0.7}_{-0.4}$	Yes	-	Yes
99	-	295.4381	40.1639	14.69	$52.2^{+0.4}_{-0.4}$	No	-	-
100	-	295.4468	40.2657	14.45	$52.9^{+2.3}_{-13.4}$	No	-	-
101	-	295.3954	40.3276	13.06	$63.1^{+1.0}_{-1.1}$	Yes	-	-
102	-	295.3926	40.3291	13.12	$31.3^{+15.0}_{-0.9}$	No	-	-
103	-	295.3621	40.3200	13.91	$22.4^{+0.2}_{-0.03}$	No	-	-
104	4936825	295.2691	40.0808	13.14	$29.5^{+2.9}_{-0.8}$	No	-	-

Table A.2. continued.

ID	KIC	RA (°)	DEC (°)	<i>Gaia</i> (mag)	ν_{\max} (μHz)	Member (this work)	S11 member	C20 member
105	5023953	295.2415	40.1382	12.59	41.9 ^{+1.8} _{-2.1}	Yes	Yes	Yes
106	5024043	295.2585	40.1078	12.78	56.7 ^{+1.6} _{-1.9}	Yes	Yes	-
107	5024268	295.2959	40.1866	11.31	19.5 ^{+6.0} _{-1.5}	No	No	Yes
108	5024297	295.3010	40.1927	12.90	34.1 ^{+13.0} _{-1.0}	No	Yes	Yes
109	5024312	295.3034	40.1915	13.54	83.9 ^{+2.7} _{-3.0}	Yes	Yes	Yes
110	5024322	295.3049	40.1116	13.09	64.2 ^{+1.4} _{-21.0}	Yes	-	No (60%)
111	5024327	295.3060	40.1989	12.75	46.6 ^{+0.6} _{-0.6}	Yes	Yes	Yes
112	5024404	295.3152	40.1696	12.86	47.4 ^{+1.9} _{-10.9}	Yes	Yes	Yes
113	5024414	295.3164	40.1865	12.65	76.4 ^{+0.2} _{-0.2}	No	Yes	Yes
114	5024456	295.3210	40.1811	11.08	142.6 ^{+0.4} _{-0.4}	No	Yes	Yes
115	5024476	295.3240	40.1544	12.51	52.2 ^{+1.6} _{-1.5}	No	Yes	Yes
116	5024512	295.3281	40.1985	13.29	60.5 ^{+13.8} _{-5.8}	Yes	Yes	Yes
117	5024517	295.3288	40.1947	13.00	38.8 ^{+5.3} _{-2.8}	No	Yes	Yes
118	5024582	295.3389	40.1992	12.67	47.2 ^{+0.6} _{-0.6}	Yes	Yes	No (30%)
119	5024583	295.3390	40.1834	12.73	32.3 ^{+5.4} _{-3.5}	Yes	Yes	Yes
120	5024601	295.3411	40.1968	12.46	29.0 ^{+12.3} _{-3.2}	Yes	Yes	Yes
121	5024750	295.3608	40.1949	11.81	11.4 ^{+0.4} _{-0.2}	Yes	Yes	Yes
122	5024967	295.3935	40.1461	12.79	48.7 ^{+3.6} _{-3.0}	Yes	Yes	Yes
123	5025021	295.4035	40.1508	12.84	47.4 ^{+0.5} _{-0.6}	Yes	-	-
124	5025101	295.4205	40.1867	13.00	23.0 ^{+0.2} _{-0.5}	No	-	-
125	5111718	295.1535	40.2548	13.80	111.4 ^{+3.1} _{-3.2}	Yes	Yes	Yes
126	5111767	295.1655	40.2312	13.64	28.3 ^{+2.2} _{-0.9}	No	-	-
127	5111940	295.2069	40.2420	13.00	55.1 ^{+6.4} _{-2.1}	Yes	Yes	Yes
128	5111949	295.2092	40.2197	12.76	39.6 ^{+1.5} _{-1.7}	Yes	Yes	Yes
129	5111987	295.2166	40.2600	14.95	87.9 ^{+2.1} _{-11.8}	No	-	-
130	5112072	295.2333	40.2276	13.74	123.8 ^{+6.3} _{-20.9}	Yes	Yes	Yes
131	5112118	295.2411	40.2314	12.59	26.3 ^{+0.9} _{-1.3}	Yes	-	-
132	5112281	295.2695	40.2476	12.18	71.9 ^{+0.6} _{-0.6}	No	-	-
133	5112361	295.2841	40.2524	13.05	74.4 ^{+1.1} _{-1.1}	Yes	No	-
134	5112373	295.2858	40.2250	12.76	43.4 ^{+0.8} _{-12.1}	Yes	Yes	Yes
135	5112387	295.2886	40.2454	12.78	40.6 ^{+1.3} _{-1.3}	Yes	Yes	Yes
136	5112401	295.2913	40.2637	12.56	39.0 ^{+0.4} _{-0.4}	Yes	Yes	Yes
137	5112403	295.2919	40.2190	13.89	20.1 ^{+1.1} _{-1.0}	No	Yes	Yes
138	5112467	295.3033	40.2066	12.76	36.1 ^{+8.1} _{-0.8}	Yes	Yes	Yes
139	5112491	295.3064	40.2057	12.71	45.2 ^{+0.5} _{-0.5}	Yes	Yes	Yes
140	5112730	295.3395	40.2326	12.72	44.0 ^{+1.3} _{-1.3}	Yes	Yes	Yes
141	5112734	295.3407	40.2031	12.80	30.9 ^{+1.2} _{-1.2}	No	Yes	Yes
142	5112744	295.3426	40.2789	12.89	43.0 ^{+0.5} _{-0.6}	Yes	Yes	Yes
143	5112880	295.3628	40.2079	12.23	22.5 ^{+1.8} _{-1.5}	Yes	Yes	Yes
144	5112938	295.3714	40.2178	12.76	44.9 ^{+2.3} _{-16.0}	Yes	Yes	Yes
145	5112948	295.3726	40.2389	12.83	32.7 ^{+9.9} _{-0.6}	No	Yes	Yes
146	5112950	295.3731	40.2058	12.71	38.6 ^{+1.0} _{-1.2}	Yes	Yes	Yes
147	5112974	295.3761	40.2560	12.64	33.6 ^{+4.1} _{-2.4}	Yes	Yes	Yes
148	5113041	295.3888	40.2097	12.79	37.1 ^{+1.1} _{-6.7}	Yes	Yes	Yes
149	5200152	295.3494	40.3623	12.67	45.5 ^{+1.0} _{-1.8}	Yes	Yes	Yes

Notes. We report whether they are cluster members following our method (this work), and whether they were determined to be cluster members in [Stello et al. 2011](#) (S11) and [Cantat-Gaudin & Anders 2020](#) (C20; only when their membership probability is 100%).